Co Nanoparticle Catalysts Encapsulated by BaO−La$_2$O$_3$ Nanofractions for Efficient Ammonia Synthesis Under Mild Reaction Conditions

Shin-ichiro Miyahara, Katsutoshi Sato,* Kotoko Tsujimaru, Yuichiro Wada, Yuta Ogura, Takaaki Toriyama, Tomokazu Yamamoto, Syo Matsumura, Koji Inazu, and Katsutoshi Nagaoka*

Read Online

ACCESS | Metrics & More | Article Recommendations | Supporting Information

ABSTRACT: Ruthenium catalysts may allow for realization of renewable energy-based ammonia synthesis processes using mild reaction conditions (<400 °C, <10 MPa). However, ruthenium is relatively rare and therefore expensive. Here, we report a Co nanoparticle catalyst loaded on a basic Ba/La$_2$O$_3$ support and prereduced at 700 °C (Co/Ba/La$_2$O$_3$_700red) that showed higher ammonia synthesis activity at 350 °C and 1.0−3.0 MPa than two benchmark Ru catalysts, Cs$^+$/Ru/MgO and Ru/CeO$_2$. The synthesis rate of the catalyst at 350 °C and 1.0 MPa (19.3 mmol h^{-1} g^{-1}) was 8.0 times that of Co/Ba/La$_2$O$_3$_500red and 6.9 times that of Co/La$_2$O$_3$_700red. The catalyst showed ammonia synthesis activity at temperatures down to 200 °C. Reduction at the high temperature induced the formation of BaO−La$_2$O$_3$ nanofractions around the Co nanoparticles by decomposition of BaCO$_3$, which increased turnover frequency, inhibited the sintering of Co nanoparticles, and suppressed ammonia poisoning. These strategies may also be applicable to other non-noble metal catalysts, such as nickel.
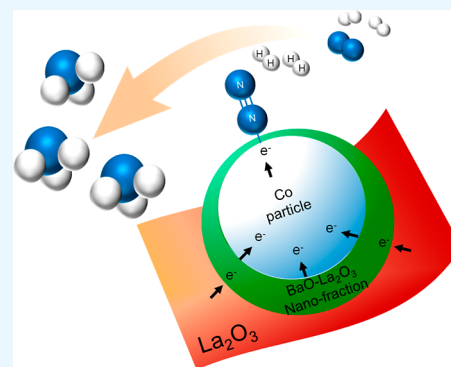
1. INTRODUCTION

Ammonia (NH$_3$) is an essential chemical feedstock in the modern chemical industry. More than 80% of the ammonia generated today is used as chemical fertilizer, and ammonia has made a huge contribution to solving the food crisis that resulted from the population explosion in the 20th century.[1−3] Recently, ammonia has attracted attention as a hydrogen and energy carrier for greater utilization of renewable energy, and as a decarbonized fuel for use in power plants and ships.[4−7] Ammonia, therefore, is considered an important material for realizing a sustainable society.

Traditionally, ammonia has been produced *via* the Haber−Bosch process. The Haber−Bosch process uses very high pressures and temperatures (>450 °C and >20 MPa) and has been highly optimized from a process engineering standpoint. However, the process uses fossil fuels as its source of hydrogen, and therefore, it emits large amounts of CO$_2$ (1.9 ton-NH$_3^{-1}$) into the atmosphere.[8] If ammonia could be produced from hydrogen produced by renewable energy, the process could be harnessed to speed up decarbonization, slow down global warming, and increase food production, which are three important current global issues.[9] A major milestone in the realization of green ammonia synthesis systems using H$_2$ produced by renewable energy is the development of catalysts that have high ammonia activity under mild conditions (<400 °C, <10 MPa).

The catalysts most commonly used in the Haber−Bosch process are Fe-based; however, these catalysts require a high temperature and pressure to dissociate the N≡N triple bond (945 kJ mol^{-1}), and, therefore, are not suitable for use in conjunction with renewable energy.[10−13] In contrast, Ru catalysts show unparalleled ammonia synthesis activity under mild conditions,[14−30] but Ru is a rather rare element that is expensive to procure. Co is cheaper and more abundant than Ru, but neat Co is less active than both Ru and Fe because the N$_2$ molecular adsorption energy of Co is lower than that of Ru and Fe.[31] As a result, previously reported oxide- or carbon-supported Co catalysts, which have the advantage of being easy to prepare and handle, show low ammonia synthesis activity under mild reaction conditions.[32−34]

As part of efforts to address this issue, we previously reported that the addition of Ba to Co/MgO and prereduction at high temperatures markedly improved the ammonia synthesis activity of the parent catalyst under mild reaction conditions (<400 °C, 1−3 MPa).[35] In fact, the resultant Co@

BaO/MgO catalyst, where the Co core is encapsulated by a strongly basic BaO shell, showed an activity that was not only higher than that of other oxide- or carbon-supported Co-based catalysts but also higher than that of active Ru catalysts, such as $Ru/La_{0.5}Ce_{0.5}O_{1.75}$ and $Cs^+/Ru/MgO$.[16,35] Spectroscopic and density functional theory investigation uncovered that the structure allows for exceptional electron donation from BaO *via* Co atoms to the antibonding π-orbital of N_2 molecules, thereby, promoting cleavage of the N≡N bond. Our findings prompted us to examine the use of other basic oxide supports, such as La_2O_3, which has higher basicity than MgO.[36,37]

Here, we report that $Co/Ba/La_2O_3$ prereduced at 700 °C showed high ammonia synthesis rates at a low reaction temperature of 350 °C: 19.3 mmol h^{-1} g^{-1} at 1.0 MPa and 35.7 mmol h^{-1} g^{-1} at 3.0 MPa. Investigations revealed that the addition of Ba and increasing the prereduction temperature from 500 to 700 °C increased the ammonia synthesis activity by 6.9 and 8 times, respectively, *via* the formation of a core (Co) - shell ($BaO-La_2O_3$) structure. The presence of BaO retarded sintering of the Co nanoparticles during high-temperature reduction. The ammonia synthesis activity—promoting effects of the addition of Ba and of increasing the reduction temperature was observed also for Ni catalysts, for which the N_2 adsorption energy of neat Ni is less than that of Co.[35] To further understand how the addition of Ba and the increase of reduction temperature affected the ammonia synthesis rate, X-ray absorption fine structure spectroscopy (XAFS), spherical aberration-corrected scanning transmission electron microscopy (Cs-STEM), and electron energy loss spectroscopy (EELS) analyses were performed on prereduced catalyst without exposure to air. In the present study, both EELS and energy-dispersive X-ray (EDX) spectrometry were used; however, EELS can distinguish between Ba and La elements, whereas EDX spectrometry cannot because, in that technique, the excitation wavelength of Ba and La are so similar that the small peak attributable to Ba overlaps the large peak attributable to La.

2. EXPERIMENTAL SECTION

2.1. Catalyst Preparation. The Ba/La_2O_3 support was prepared by a precipitation and impregnation method as follows. First, a suspension of La hydroxides was formed by dropping an aqueous solution of $La(NO_3)_3\cdot6H_2O$ (Wako Pure Chemical, Japan) into a 28 wt % solution of aqueous ammonia (Wako Pure Chemical). The La hydroxides were collected by filtration, washed with distilled water, and added to an aqueous solution containing $Ba(OH)_2\cdot8H_2O$ (Wako Pure Chemical). The amount of Ba was fixed at $Ba/(Ba + La) = 0.05$ mol/mol. After stirring the suspension for 1 h, the aqueous solvent was removed by rotary evaporation. The resulting powder was calcined at 700 °C in static air and used as the catalyst support.

Next, Co was loaded onto the support. Bis(2,4-pentanedionate)cobalt(II) dihydrate (Tokyo Chemical Industry, Japan) dissolved in tetrahydrofuran (Wako Pure Chemical) was used as the Co precursor. The support was added to the dissolved precursor, and the suspension was stirred overnight. When the stirring was finished, the tetrahydrofuran was removed by rotary evaporation, leaving behind a powder that was then heated to 500 °C under an Ar flow. The Co loading was fixed at 20 wt % for each catalyst. Two benchmark Ru catalysts (Ru/CeO_2 and $Cs^+/Ru/MgO$) were also prepared as reported by us previously.[14,37]

2.2. Ammonia Synthesis Activity Test. The rate of ammonia synthesis over the catalysts was measured by using 100 mg of catalyst and a conventional flow system with a tubular reactor under either atmospheric pressure or high pressure, as reported previously.[38] Research-grade gases (>99.99%) were supplied from high-pressure cylinders and purified with a gas purifier (Micro Torr MC50-904FV, SAES Pure Gas, US). The catalysts were prereduced *in situ* with pure H_2 (60 mL min^{-1}) at 500, 700, or 800 °C for 1 h at 0.1 MPa and then cooled at 300 °C in an Ar stream. The pressure was then adjusted to 0.1, 1.0, or 3.0 MPa. A mixture of N_2 (30 mL min^{-1}) and H_2 (90 mL min^{-1}) was then passed over the catalyst (space velocity = 72,000 mL h^{-1} g^{-1}). The produced ammonia gas was trapped in an aqueous solution of H_2SO_4, and the rate of ammonia synthesis was calculated from the decrease in the electron conductivity of the H_2SO_4 aqueous solution, which was monitored with an electron conductivity detector (CM-30R, DKK-TOA, Japan).

2.3. Kinetic Analysis. Reaction kinetics were analyzed as previously reported.[35,39,40] The reaction orders with respect to N_2, H_2, and NH_3 were calculated by measuring the N_2, H_2, and NH_3 pressure dependence of the NH_3 synthesis rate and by assuming that the rate of the reaction (r) could be described by the following expression

$$r = kP_{N_2}^n P_{H_2}^h P_{NH_3}^a$$

2.4. Characterization. High-angle annular dark-field scanning transmission electron microscope (HAADF-STEM) images, EDX elemental maps, and EELS spectra were obtained with an aberration-corrected electron microscope (JEM-ARM200CF, JEOL, Japan). The scanning transmission electron microscopy observations were conducted at 120 kV to reduce damage to the sample by the electron beam. Catalyst samples were prereduced at 500 or 700 °C under a H_2 flow and then crushed and powdered. Samples of the powdered catalyst were then placed on transmission electron microscopy grids in a glovebox. The grids were then transferred by means of a special holder with a gas cell from the glovebox to the inside of the transmission electron microscopy column without being exposed to air. For the other observations, samples were dispersed in ethanol under ambient conditions, and samples of the dispersion were dropped onto a carbon-coated copper grid and dried under a vacuum at ambient temperature for 24 h.

The specific surface area of the catalysts was measured by using the Brunauer−Emmett−Teller method. Test samples were pretreated at 300 °C in a vacuum, and the amount of N_2 adsorbed was measured with a BELSORP-mini gas adsorption instrument (BEL Japan, Inc., Japan).

H_2 chemisorption capacity was measured with a BELCAT-B apparatus (MicrotracBEL, Japan) using the same method as in the previous report.[35] H_2 was fed to a 100 mg sample of catalyst at 60 mL min^{-1}, and the temperature was increased at a rate of 10 °C min^{-1} from room temperature to 500, 700, or 800 °C. The sample was maintained at the desired temperature for 60 min in the H_2 flow; it was then purged with a stream of Ar (60 mL min^{-1}) for 30 min, cooled to 35 °C, and flushed with Ar for 60 min. After pretreatment, the H_2 chemisorption measurement was carried out at 35 °C.

XAFS measurements of the Co K-edges were performed on the BL5S1 beamline at Aichi Synchrotron Radiation Center (Aichi, Japan).

X-ray diffraction (XRD) analysis was performed with a SmartLab X-ray diffractometer (Rigaku, Japan) equipped with a Cu Kα radiation source. The XRD patterns were analyzed by using the PDXL2 software (Rigaku) and three databases (International Centre for Diffraction Data database, Crystallography Open Database, and AtomWork database).

Temperature-programed reduction measurements were performed under a flow of 100% H$_2$ using a BEL-CAT-II apparatus (MicrotracBEL). The flow rate of the gas was 60 mL min^{-1}. A 100 mg sample of catalyst was heated from 25 to 1000 °C at a rate of 10 °C min^{-1}. The CH$_4$, H$_2$O, CO, and CO$_2$ profiles were monitored by a quadruple mass spectrometer at m/z = 16, 18, 28, and 44, respectively.

3. RESULTS AND DISCUSSION

3.1. Ammonia Synthesis Activity. First, we examined the influence of reduction temperature (500−800 °C) on the NH$_3$ synthesis rate of the Co/Ba/La$_2$O$_3$ catalyst (Figure 1). The
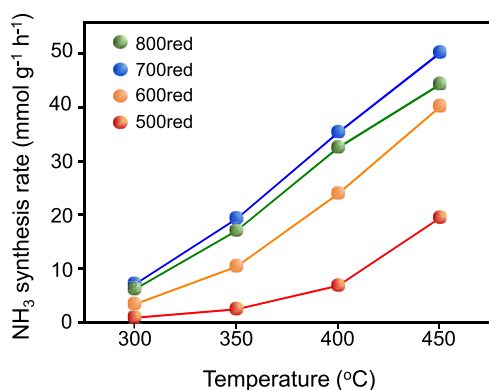
Figure 1. Influence of reduction temperature on the NH$_3$ synthesis rate of Co/Ba/La$_2$O$_3$ at 1.0 MPa.

catalyst prereduced at 500 °C (designated Co/Ba/La$_2$O$_3$_500red) showed little NH$_3$ synthesis activity at 300 °C, but the activity increased with increasing reaction temperature until a moderate activity was obtained at 450 °C. Compared with Co/Ba/La$_2$O$_3$_500red, Co/Ba/La$_2$O$_3$_600red and Co/Ba/La$_2$O$_3$_700red both showed greater NH$_3$ synthesis activity across the whole reaction temperature range examined, and Co/Ba/La$_2$O$_3$_800red showed an

activity between that of Co/Ba/La$_2$O$_3$_600red and Co/Ba/La$_2$O$_3$_700red. Ea is the apparent activation energy calculated from Arrhenius plots of the ammonia synthesis rate in the temperature range of 300−375 °C under 1.0 MPa. The apparent activation energy of the Co/Ba/La$_2$O$_3$ catalyst was found to decrease from 73.1 to 45.7 kJ mol^{-1} as the reduction temperature was increased from 500 to 700 °C (Figure S1). Furthermore, Co/Ba/La$_2$O$_3$_700red was found to have ammonia synthesis activity at reaction temperatures as low as 200 °C (synthesis rate, 0.3 mmol h^{-1} g^{-1}; Figure S2). Then, we studied the influence of Co loading and Ba content (Figures S3 and S4). The optimal amount of Co loading was 20 wt % and Ba content was 5 mol %. Furthermore, it must be mentioned that the Co precursor study showed that Bis(2,4-pentanedionate)cobalt(II) dihydrate was better than cobalt (II) nitrate hexahydrate (Figure S5).

Next, we examined the effect of adding Ba on the NH$_3$ synthesis rate of different Co and Ni catalysts (Figure 2). At a reaction temperature of 350 °C, the NH$_3$ synthesis rate of Co/Ba/La$_2$O$_3$_700red was 19.3 mmol h^{-1} g^{-1}, which was 8.0 times that of Co/Ba/La$_2$O$_3$_500red and 6.9 times that of Co/La$_2$O$_3$_700red at the same temperature. Despite the activity of Co/Ba/La$_2$O$_3$_700red being slightly lower than that of Co/Ba/MgO_700red, its activity was comparable with those reported for other state-of-the-art Co catalysts, such as Co/BaCeO$_{3-x}$N$_y$H$_z$,[41] BaH$_2$−Co/CNTs,[42] and LaCoSi,[43] notwithstanding the different Co loadings, reaction pressures, and space velocities used in the previously reported studies (Table S1). For the Ni catalysts, reduction at high temperature and the addition of Ba were also found to have positive effects on NH$_3$ synthesis activity: the fact that the NH$_3$ synthesis rate of Ni/Ba/La$_2$O$_3$_700red was much higher than those of Ni/Ba/La$_2$O$_3$_500red and Ni/La$_2$O$_3$_700red at all temperatures suggested the possibility of activating Ni by using the same strategy used to activate Co.

We also examined the effect of reaction pressure on the NH$_3$ synthesis rate at 350 °C and compared the rates with Co/Ba/La$_2$O$_3$_700red to those with the two benchmark Ru catalysts, Cs$^+$/Ru/MgO and Ru/CeO$_2$ (Figure 3). Cs$^+$/Ru/MgO is a well-known Ru catalyst with high NH$_3$ synthesis activity.[44−47] Ru/CeO$_2$ is a candidate catalyst for use in ammonia synthesis processes that use renewable energy.[48] At 0.1 MPa, the NH$_3$ synthesis rate of Co/Ba/La$_2$O$_3$_700red was lower than those
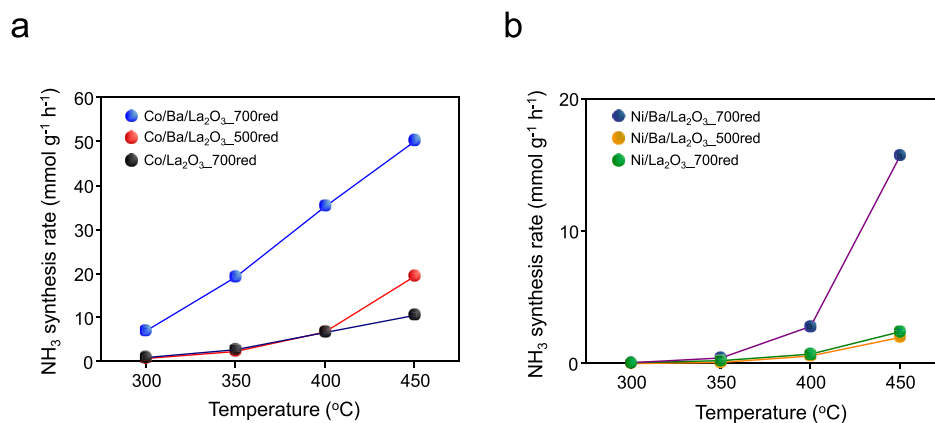
Figure 2. Temperature dependence of the NH$_3$ synthesis activities of supported Co and Ni catalysts at 1.0 MPa. The catalysts were prereduced at 500 and 700 °C (Co/Ba/La$_2$O$_3$_T red, T represents the prereduced temperature of the catalyst). (a) Supported Co catalysts. (b) Supported Ni catalysts.
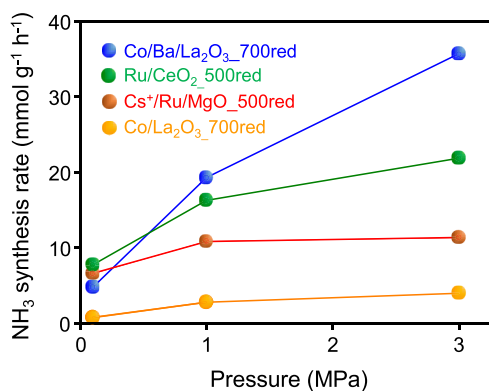
Figure 3. Pressure dependence of the NH_3 synthesis activities of Co/Ba/La_2O_3_700red, Co/La_2O_3_700red, and the two benchmark Ru catalysts at 350 °C.

of Cs^+/Ru/MgO_500red and Ru/CeO_2_500red. However, when the reaction pressure was increased, the NH_3 synthesis rate of Co/Ba/La_2O_3_700red increased drastically, whereas those of the two Ru catalysts increased only slightly. As a result, the NH_3 synthesis rate of Co/Ba/La_2O_3_700red at 1.0 and at 3.0 MPa exceeded the rates of the two benchmark catalysts (synthesis rate at 3.0 MPa: Co/Ba/La_2O_3_700red, 35.7 mmol h^{-1} g^{-1}; Ru/CeO_2_500red, 13.7 mmol h^{-1} g^{-1}; and Cs^+/Ru/MgO_500red, 11.4 mmol h^{-1} g^{-1}). We also examined the NH_3 synthesis rate of Co/La_2O_3_700red and found that it was much lower than the rates of the other catalysts at all pressures.

To investigate the cause of the different pressure dependences, we performed a kinetic analysis at 350 °C and 0.1 MPa using the same four catalysts (Table 1 and Figures S6 and S7).

Table 1. Results of a Kinetic Analysis Over Cs^+/Ru/MgO, Ru/CeO_2, Co/Ba/La_2O_3, or Co/La_2O_3

	order[a]		
catalyst	n^a	h^b	a^c
Cs^+/Ru/MgO_500red	1.07	−0.76	−0.15
Ru/CeO_2_500red	0.85	−0.18	−0.19
Co/Ba/La_2O_3_700red	0.85	0.43	−0.17
Co/La_2O_3_700red	0.97	0.32	−0.51

[a]Reaction order with respect to N_2. [b]Reaction order with respect to H_2. [c]Reaction order with respect to NH_3.

The fact that the reaction order with respect to N_2 was almost unity for all of the catalysts indicated that the rate-determining step was the dissociation of molecular N_2. However, the fact that the reaction order with respect to H_2 was −0.18 and −0.76 for Ru/CeO_2_500red and Cs^+/Ru/MgO_500red, respectively, indicated that H atoms strongly adsorbed onto the Ru surface and inhibited activation of molecular N_2; this is

referred to as hydrogen poisoning and is a typical drawback of Ru catalysts. In contrast, the positive reaction orders with respect to H_2, +0.43 and +0.32, that were obtained for Co/Ba/La_2O_3_700red and Co/La_2O_3_700red, respectively, indicated that these catalysts were free from hydrogen poisoning and that N_2 activation was promoted with increasing hydrogen pressure. A large negative reaction order with respect to NH_3 (−0.51) was obtained for Co/La_2O_3_700red, but this value was reduced to −0.17 with the addition of Ba. These findings suggest that it is difficult for the ammonia yield of Co/La_2O_3_700red to approach the equilibrium value because adsorbed NH, NH_2, and NH_3 inhibit the reaction. However, the addition of Ba can be expected to promote the desorption of such adsorbates and thus accelerate the reaction, even near equilibrium. Together, these results indicate that Co catalysts may be a viable alternative to Ru catalysts.

3.2. Effects of Doping with Ba. To understand more about the effects of Ba doping, we compared the physicochemical properties of Co/Ba/La_2O_3_700red and Co/La_2O_3_700red (Table 2). The specific surface areas of the two catalysts were comparable, but the mean Co particle size, as measured by STEM, was much smaller for Co/Ba/La_2O_3_700red than for Co/La_2O_3_700red (20 nm vs 70 nm). The indication was that the addition of Ba inhibited the sintering of the Co particles during reduction. Assuming the Co particles were cubic, this difference in particle size corresponds to 3.5-times greater Co dispersion for Co/Ba/La_2O_3_700red compared with Co dispersion for Co/La_2O_3_700red. On the other hand, the H_2 chemisorption value (a measure of the Co dispersion) of Co/Ba/La_2O_3_700red was found to be only 1.6-times greater than that of Co/La_2O_3_700red. The indication was that the surface of the Co particles in Co/Ba/La_2O_3_700red was partly covered by the support material. Also, the turnover frequency (TOF) of Co/Ba/La_2O_3_700red was about 4.4 times that of Co/La_2O_3_700red. Together, these results indicate that the drastic increase in NH_3 synthesis rate observed as a result of doping with Ba was the combined result of inhibition of Co particle sintering and an increase of TOF.

To understand how doping with Ba affected the state of the Co, we subjected Co/Ba/La_2O_3_700red and Co/La_2O_3_700red to XANES analysis (Figure 4). The fact that the Co K-edge XANES spectra of the two catalysts were comparable with that of Co foil indicated that the Co atoms in the catalysts were fully reduced to a metallic state after reduction at 700 °C.

Next, we investigated the morphology of Co/Ba/La_2O_3_700red by means of Cs-STEM and EELS. To avoid any unwanted structural or state changes, we used a special holder with a gas cell that allowed the sample to be transferred from the reactor to the STEM apparatus under an inert gas environment.[35] HAADF-STEM images revealed that the Co

Table 2. Physicochemical Properties and Catalytic Performances of Supported Co Catalysts

catalyst	SSA[a] [m^2 g_{cat}^{-1}]	H_2 chemisorption[b] [μmol g^{-1}]	d^c [nm]	rate[d] [mmol g_{cat}^{-1} h^{-1}]	TOF[e] [s^{-1}]
Co/Ba/La_2O_3_500red	37.5	35.0	10	2.4	0.019
Co/Ba/La_2O_3_700red	24.9	24.1	20	19.3	0.223
Co/Ba/La_2O_3_800red	10.1	15.6	34	17.1	0.304
Co/La_2O_3_700red	25.8	14.9	70	2.8	0.051

[a]Specific surface area. [b]Measured using H_2 chemisorption capacity. [c]Mean particle size of Co nanoparticles, as estimated by Cs-STEM (see Figures S8−S11). [d]At 350 °C and 1.0 MPa. [e]TOF. Calculated from the H_2 chemisorption value and the NH_3 synthesis rate (see Table 2).
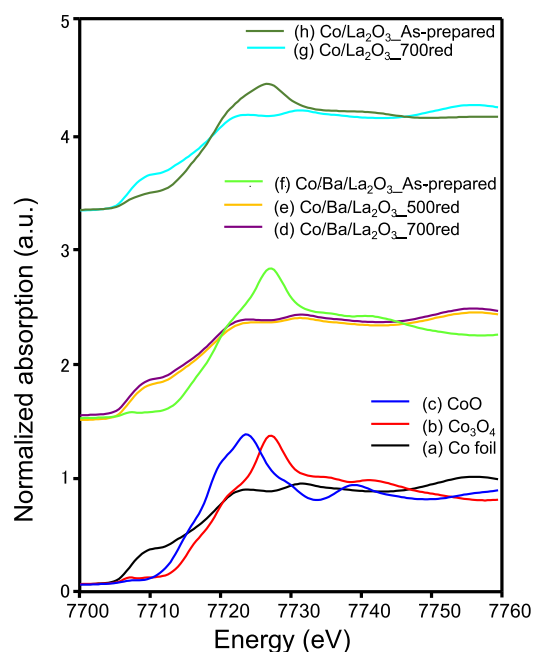
Figure 4. Normalized Co K-edge XANES spectra for Co/La$_2$O$_3$ and Co/Ba/La$_2$O$_3$ catalysts prereduced at different temperatures, and for several reference samples.

particles were encapsulated by a 2−3 mm-thick nanofraction (Figures 5a and S10). EELS mapping revealed that Ba and La elements were enriched in the nanofraction (Figures 5b,c,e and 4d). Although a low abundance of Ba was included overall in the catalyst (Ba/La molar ratio, 5:95), a high abundance of Ba was observed in the nanofraction. In contrast, the fact that the carbon element was not detected in the nanofraction (Figure 5f−h) indicated that the nanofraction was an oxide or hydroxide of Ba or La. Morphology of the catalyst as well as NH$_3$ synthesis rate was maintained during the 50 h of reaction (Figures S12 and S13).

3.3. Effect of the Reduction Temperature. Finally, to understand the effects of the reduction temperature on Co/Ba/La$_2$O$_3$, we investigated the physicochemical properties of the catalyst after reduction at different temperatures. With the increase in reduction temperature from 500 to 700 to 800 °C, the specific surface area decreased from 37.5 to 24.9 to 10.1 m^2 g^{-1}, and the mean diameter of the Co particles increased from 10 to 20 to 34 nm. The indication was that greater sintering occurred at higher reduction temperatures (Table 2). It must be noted that the fact that the mean Co particle size was comparable both before and after exposure of Co/Ba/La$_2$O$_3$_700red to air indicated that exposure to air had no effect on Co particle size (see Figures 5 and S10, S14). Also, the number of exposed Co particles decreased and the TOF drastically increased from 0.019 to 0.223 to 0.304 with the increasing reduction temperature.

To understand why the TOF after reduction at 700 °C was more than 12 times that after reduction at 500 °C, we conducted a detailed characterization of the catalysts. First, to investigate the state of Co, we measured Co K-edge XANES spectra in as-prepared Co/Ba/La$_2$O$_3$ and Co/Ba/La$_2$O$_3$ prereduced at different temperatures (Figure 4). The fact that the spectra for Co/Ba/La$_2$O$_3$_500red and Co/Ba/La$_2$O$_3$_700red were comparable to that for Co foil indicated that inactive oxidic Co was reduced to the metallic state after

reduction at ≥500 °C and that difference of the TOF was not ascribed to the difference of the Co reduction degree.

To investigate the surface state of Co/Ba/La$_2$O$_3$_500red, we performed Cs-STEM and EELS observations without exposing the catalyst to the air (Figures 6 and S15). In contrast to the findings for Co/Ba/La$_2$O$_3$_700red (Figures 5 and S14), the Co particles in Co/Ba/La$_2$O$_3$_500red were not well crystallized and were partially surrounded by a cloud-like substance containing Ba, La, and carbon elements. The fact that carbon element was observed in parts of the cloud in Co/Ba/La$_2$O$_3$_500red indicated the presence of noncrystallized carbonate species of Ba and or La because crystallized carbonate species was not observed by XRD analysis (Figure S16). Recall that such elemental carbon was not observed for Co/Ba/La$_2$O$_3$_700red by EELS measurement (Figures 5 and S14). Carbonate species, due to their acidity, decrease the ability of the support material to donate electrons. Therefore, we concluded that one of the causes of the high TOF of Co/Ba/La$_2$O$_3$_700red was the complete removal of La and Ba carbonate species during reduction at high temperatures. It is likely that hydroxide species are also removed from the catalyst because the temperature-programed reduction profile of fresh Co/Ba/La$_2$O$_3$ indicated that the formation of CH$_4$, CO, CO$_2$, and H$_2$O was completed at a temperature below 700 °C (Figure 7). Thus, these data indicated that the low crystalline nanofraction encapsulating the Co nanoparticles in Co/Ba/La$_2$O$_3$_700red was composed of BaO and La$_2$O$_3$. Therefore, another of the causes of the high TOF of Co/Ba/La$_2$O$_3$_700red was ascribed to encapsulation of the Co particles by the low crystalline nanofraction of BaO−La$_2$O$_3$. Previously, based on density functional theory calculations and Fourier-transform infrared spectroscopy measurements after adsorption of molecular N$_2$ on the catalyst, we reported the high activity of Co nanoparticles encapsulated by BaO loaded on MgO (Co@BaO/MgO), which we ascribed to strong electron donation from BaO to N$_2$ via Co.[35] Although in the present study we were unable to fabricate a self-supporting disk of the Co/Ba/La$_2$O$_3$ catalyst that transmitted infrared light and therefore could not use Fourier-transform infrared spectroscopy, the high TOF of Co/Ba/La$_2$O$_3$_700red may also be due to such electron donation from BaO−La$_2$O$_3$ to the antibonding π-orbital of the N≡N bond of molecular N$_2$. We also found that increasing the reduction temperature up to 800 °C further increased the TOF due to the growth of low crystalline nanofractions on Co nanoparticles; however, the NH$_3$ synthesis rate decreased due to the sintering of the Co particles (Table 2).

Here we address the formation mechanism of the core (Co) - shell (BaO−La$_2$O$_3$) structure which is almost identical to the formation mechanism of the core (Co) - shell (BaO) structure on MgO.[35] As already discussed, a majority of Ba in the as-prepared catalyst exists as BaCO$_3$. The decomposition reaction of BaCO$_3$ proceeds as follows to produce BaO.

$$BaCO_3 + 4H_2 \rightarrow BaO + CH_4 + 2H_2O$$
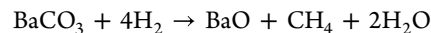
During this decomposition, Ba(OH)$_2$ can form and decompose to BaO. Compared with their Mg counterparts, Ba compounds usually have lower melting points, allowing them to melt and travel across the catalyst surface during reduction at high temperatures. Similarly, Co nanoparticles, which contain metallic Co formed from the reduction of Co oxide, also move across the support surface and become sintered. While mobile, these Co nanoparticles collect the Ba
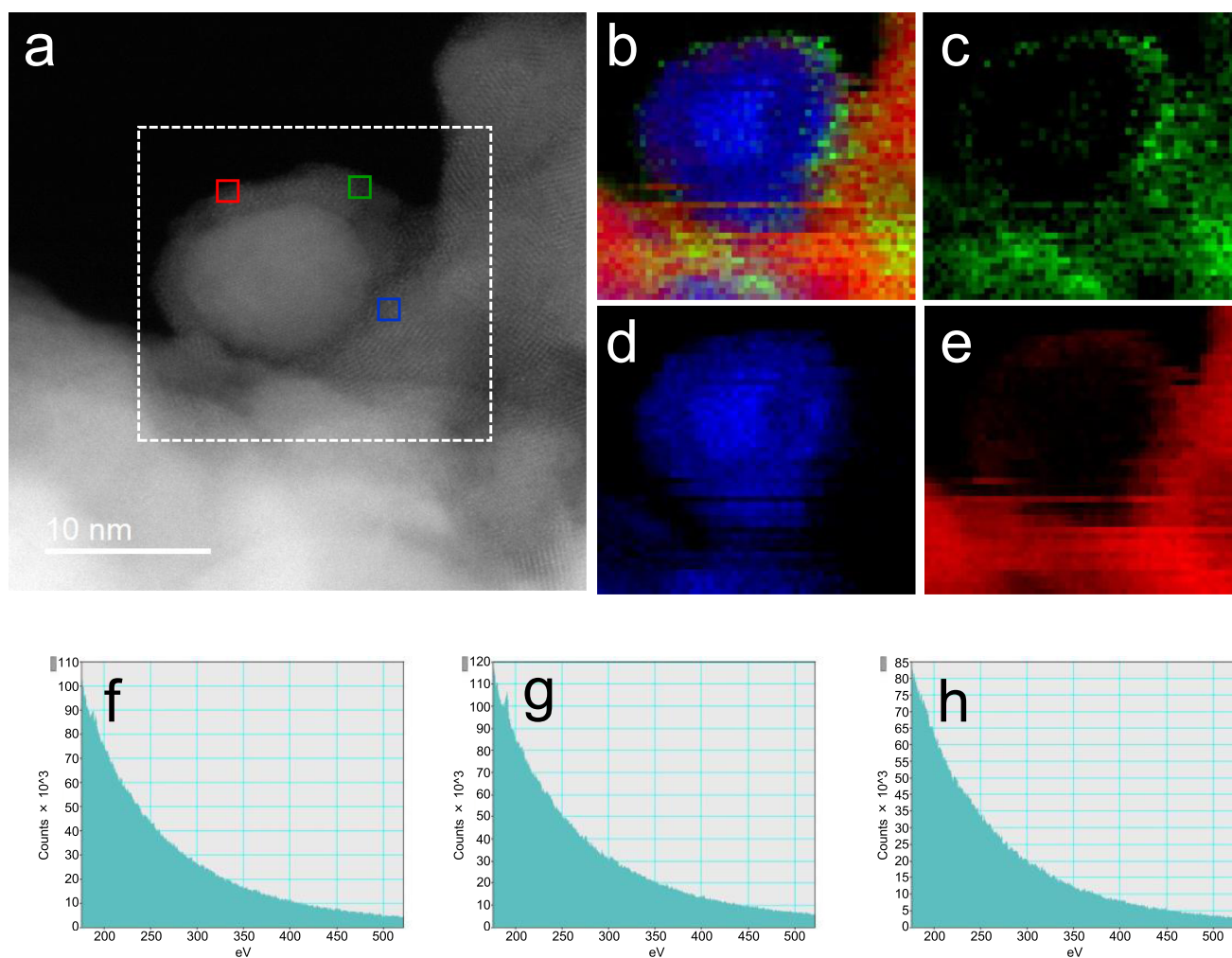
Figure 5. HAADF-STEM image and electron energy loss spectroscopy maps of Co/Ba/La$_2$O$_3$_700red without exposure to air. (a) HAADF-STEM image of the catalyst. (b−e) Electron energy loss spectroscopy maps of (b) overlay, (c) Ba L, (d) Co L, and (e) La L in the area within the white, dotted square in (a). (f−h) C K electron energy loss spectroscopy spectra of the areas indicated by the green (f), blue (g), and red (h) squares in (a).

compound, which results in a reduction of the surface energy of the Co nanoparticles. In the present catalyst, Ba(OH)$_2$ melts at low temperature (melting point, 408 °C), migrates with La$_2$O$_3$ to the Co nanoparticle surface, and then decomposes to BaO with a high melting point (1920 °C). This BaO then coagulates between BaO−La$_2$O$_3$ and BaO−La$_2$O$_3$ and between BaO−La$_2$O$_3$ and Co nanoparticles as a nanofraction containing voids through which gases can pass.

Co/Ba/La$_2$O$_3$_700red and Co@Ba/MgO_700red[35] showed comparable TOFs, but the NH$_3$ synthesis rate (350 °C, 1 MPa) of Co@Ba/MgO_700red was 1.3 times that of Co/Ba/La$_2$O$_3$_700red. These results indicated that, fundamentally, the core (Co) - shell (BaO−La$_2$O$_3$) structure enhanced the NH$_3$ synthesis ability of surface Co, and that the difference in NH$_3$ synthesis rate between these catalysts was due to the difference in the mean Co particle size (i.e., 10.6 *vs* 20 nm for Co@Ba/MgO_700red and Co/Ba/La$_2$O$_3$_700red). The higher surface area of Co@Ba/MgO_700red (47.6 m^2 g^{-1}) compared with that of Co/Ba/La$_2$O$_3$_700red likely contributed to the formation of fine Co nanoparticles. Thus, the use of a basic support with a higher specific surface area is expected to afford catalysts with enhanced NH$_3$ synthesis rates.

4. CONCLUSIONS

Here, by encapsulating Co nanoparticles within BaO−La$_2$O$_3$ on a La$_2$O$_3$ support, we constructed a catalyst that showed high NH$_3$ synthesis activity even under mild reaction conditions. The Co/Ba/La$_2$O$_3$ prereduced at 700 °C showed high NH$_3$ synthesis activity with a synthesis rate of 19.3 mmol h^{-1} g^{-1} at 350 °C, which was 6.9 times that of the nondoped parent catalyst. Moreover, the Co/Ba/La$_2$O$_3$ prereduced at 700 °C was active at temperatures down to 200 °C. We also found that the addition of Ba to the catalyst inhibited the sintering of the Co particles during reduction. Increasing the reduction temperature from 500 to 700 °C resulted in a drastic increase in TOF from 0.019 to 0.223. The increase in TOF was ascribed to the encapsulation of Co particles by a BaO−La$_2$O$_3$ nanofraction during high-temperature reduction. It is likely that donation of electrons from the nanofraction to molecular N$_2$ *via* Co markedly promoted NH$_3$ synthesis. Furthermore, the elimination of ammonia poisoning by the addition of Ba is a potential merit for carrying out the reaction near equilibrium. The present findings also indicate that these strategies are also likely applicable to Ni catalysts. Together, the present results provide information that will be useful for the development of highly active NH$_3$ synthesis catalysts for use in processes that
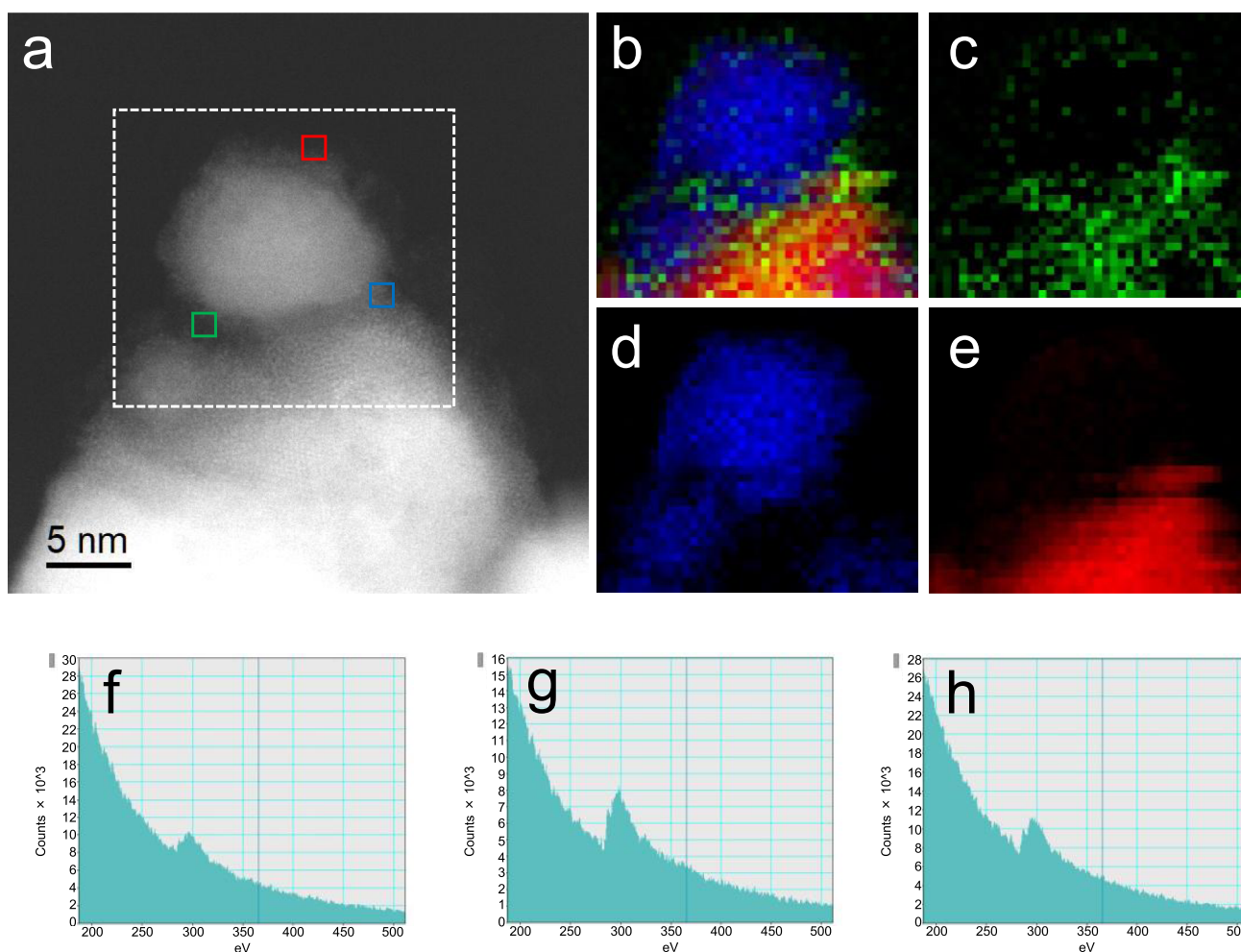
Figure 6. HAADF-STEM image and electron energy loss spectroscopy maps of Co/Ba/La$_2$O$_3$_500red without exposure to air. (a) HAADF-STEM image of the catalyst. (b−e) Electron energy loss spectroscopy maps of (b) overlay, (c) Ba L, (d) Co L, and (e) La L in the area within the white, dotted square in (a). (f−h) C K electron energy loss spectroscopy spectra of the areas indicated by the green (f), blue (g), and red (h) squares in (a).
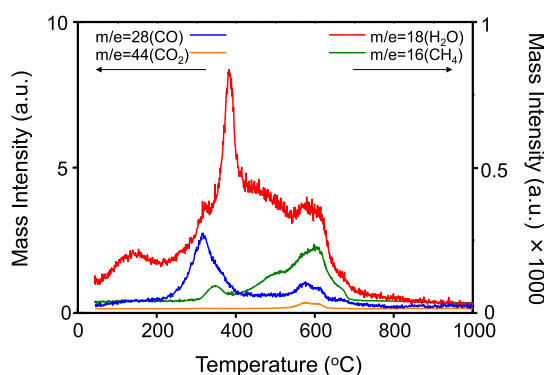

Figure 7. H$_2$-temperature-programed reduction profiles for the as-prepared Co/Ba/La$_2$O$_3$ catalyst.

use renewable energy. Such catalysts are expected to play a major role in the realization of a carbon-neutral society.

■ ASSOCIATED CONTENT

Ⓢ Supporting Information

The Supporting Information is available free of charge at https://pubs.acs.org/doi/10.1021/acsomega.2c01973.

Detailed procedures and data for kinetic analysis; Arrhenius plots; influence of reaction temperature at low temperature; influence of Co loading; influence of Ba content; influence of Co precursor; additional STEM images; time course of ammonia synthesis rate; XRD pattern; and summary of the ammonia synthesis activity over various Co-based catalysts (PDF)

■ AUTHOR INFORMATION

Corresponding Authors

Katsutoshi Sato − *Department of Chemical Systems Engineering, Graduate School of Engineering, Nagoya University, Nagoya 464-8603, Japan;* ⓞ orcid.org/0000-0002-3998-7012; Email: sato.katsutoshi@marerial.nagoya-u.ac.jp

Katsutoshi Nagaoka − *Department of Chemical Systems Engineering, Graduate School of Engineering, Nagoya University, Nagoya 464-8603, Japan;* ⓞ orcid.org/0000-0003-1774-1537; Email: nagaoka.katsutoshi@material.nagoya-u.ac.jp

Authors

Shin-ichiro Miyahara — *Department of Chemical Systems Engineering, Graduate School of Engineering, Nagoya University, Nagoya 464-8603, Japan*

Kotoko Tsujimaru — *Department of Integrated Science and Technology, Faculty of Science and Engineering, Oita University, Oita 870−1192, Japan*

Yuichiro Wada — *Department of Integrated Science and Technology, Faculty of Science and Engineering, Oita University, Oita 870−1192, Japan*

Yuta Ogura — *Department of Chemical Systems Engineering, Graduate School of Engineering, Nagoya University, Nagoya 464-8603, Japan*

Takaaki Toriyama — *The Ultramicroscopy Research Center, Kyushu University, Fukuoka 819-0395, Japan*

Tomokazu Yamamoto — *Department of Applied Quantum Physics and Nuclear Engineering, Kyushu University, Fukuoka 819-0395, Japan*

Syo Matsumura — *The Ultramicroscopy Research Center, Kyushu University, Fukuoka 819-0395, Japan; Department of Applied Quantum Physics and Nuclear Engineering, Kyushu University, Fukuoka 819-0395, Japan*

Koji Inazu — *National Institute of Technology, Numazu College, Shizuoka 410-8501, Japan*

Complete contact information is available at:
https://pubs.acs.org/10.1021/acsomega.2c01973

Author Contributions

Funding

Notes

■ REFERENCES

(1) Erisman, J. W.; Sutton, M. A.; Galloway, J.; Klimont, Z.; Winiwarter, W. How a century of ammonia synthesis changed the world. *Nat. Geosci.* **2008**, *1*, 636−639.

(2) Smil, V. Detonator of the population explosion. *Nature* **1999**, *400*, 415.

(3) Galloway, J. N.; Townsend, A. R.; Erisman, J. W.; Bekunda, M.; Cai, Z.; Freney, J. R.; Martinelli, L. A.; Seitzinger, S. P.; Sutton, M. A. Transformation of the nitrogen cycle: Recent trends, questions, and potential solutions. *Science* **2008**, *320*, 889−892.

(4) Kandemir, T.; Schuster, M. E.; Senyshyn, A.; Behrens, M.; Schlögl, R. The Haber-Bosch Process Revisited: On the Real Structure and Stability of "Ammonia Iron" under Working Conditions. *Angew. Chem., Int. Ed.* **2013**, *52*, 12723−12726.

(5) Schlögl, R. Catalytic synthesis of ammonia - A "never-ending story". *Angew. Chem., Int. Ed.* **2003**, *42*, 2004−2008.

(6) Service, R. F. Liquid Sunshine. *Science* **2018**, *361*, 120−123.

(7) Smith, C.; Hill, A. K.; Torrente-Murciano, L. Current and future role of Haber-Bosch ammonia in a carbon-free energy landscape. *Energy Environ. Sci.* **2020**, *13*, 331−344.

(8) Rafiqul, I.; Weber, C.; Lehmann, B.; Voss, A. Energy efficiency improvements in ammonia production - perspectives and uncertainties. *Energy* **2005**, *30*, 2487−2504.

(9) Miura, D.; Tezuka, T. A comparative study of ammonia energy systems as a future energy carrier, with particular reference to vehicle use in Japan. *Energy* **2014**, *68*, 428−436.

(10) Pool, J. A.; Lobkovsky, E.; Chirik, P. J. Hydrogenation and cleavage of dinitrogen to ammonia with a zirconium complex. *Nature* **2004**, *427*, 527−530.

(11) Foster, S. L.; Bakovic, S. I. P.; Duda, R. D.; Maheshwari, S.; Milton, R. D.; Minteer, S. D.; Janik, M. J.; Renner, J. N.; Greenlee, L. F. Catalysts for nitrogen reduction to ammonia. *Nat. Catal.* **2018**, *1*, 490−500.

(12) Chae, H. K.; Siberio-Perez, D. Y.; Siberio-Pérez, D. Y.; Kim, J.; Go, Y.; Eddaoudi, M.; Matzger, A. J.; O'Keeffe, M.; Yaghi, O. M. A route to high surface area, porosity and inclusion of large molecules in crystals. *Nature* **2004**, *427*, 523−527.

(13) Gambarotta, S.; Scott, J. Multimetallic cooperative activation of N-2. *Angew. Chem., Int. Ed.* **2004**, *43*, 5298−5308.

(14) Sato, K.; Miyahara, S.-i.; Ogura, Y.; Tsujimaru, K.; Wada, Y.; Toriyama, T.; Yamamoto, T.; Matsumura, S.; Nagaoka, K. Surface Dynamics for Creating Highly Active Ru Sites for Ammonia Synthesis: Accumulation of a Low-Crystalline, Oxygen-Deficient Nanofraction. *ACS Sustainable Chem. Eng.* **2020**, *8*, 2726−2734.

(15) Hill, A. K.; Torrente-Murciano, L. Low temperature H-2 production from ammonia using ruthenium-based catalysts: Synergetic effect of promoter and support. *Appl. Catal., B* **2015**, *172−173*, 129−135.

(16) Ogura, Y.; Sato, K.; Miyahara, S.-i.; Kawano, Y.; Toriyama, T.; Yamamoto, T.; Matsumura, S.; Hosokawa, S.; Nagaoka, K. Efficient ammonia synthesis over a $Ru/La_{0.5}Ce_{0.5}O_{1.75}$ catalyst pre-reduced at high temperature. *Chem. Sci.* **2018**, *9*, 2230−2237.

(17) Kitano, M.; Inoue, Y.; Yamazaki, Y.; Hayashi, F.; Kanbara, S.; Matsuishi, S.; Yokoyama, T.; Kim, S.-W.; Hara, M.; Hosono, H. Ammonia synthesis using a stable electride as an electron donor and reversible hydrogen store. *Nat. Chem.* **2012**, *4*, 934−940.

(18) Sato, K.; Nagaoka, K. Boosting Ammonia Synthesis under Mild Reaction Conditions by Precise Control of the Basic Oxide-Ru Interface. *Chem. Lett.* **2021**, *50*, 687−696.

(19) Kobayashi, Y.; Tang, Y.; Kageyama, T.; Yamashita, H.; Masuda, N.; Hosokawa, S.; Kageyama, H. Titanium-Based Hydrides as Heterogeneous Catalysts for Ammonia Synthesis. *J. Am. Chem. Soc.* **2017**, *139*, 18240−18246.

(20) Kitano, M.; Inoue, Y.; Sasase, M.; Kishida, K.; Kobayashi, Y.; Nishiyama, K.; Tada, T.; Kawamura, S.; Yokoyama, T.; Hara, M.; Hosono, H. Self-organized Ruthenium-Barium Core-Shell Nanoparticles on a Mesoporous Calcium Amide Matrix for Efficient Low-Temperature Ammonia Synthesis. *Angew. Chem., Int. Ed.* **2018**, *57*, 2648−2652.

(21) Hattori, M.; Iijima, S.; Nakao, T.; Hosono, H.; Hara, M. Solid solution for catalytic ammonia synthesis from nitrogen and hydrogen gases at 50 degrees C. *Nat. Commun.* **2020**, *11*, 1.

(22) Wang, S. J.; Yin, S. F.; Li, L.; Xu, B. Q.; Ng, C. F.; Au, C. T. Investigation on modification of Ru/CNTs catalyst for the generation of COx-free hydrogen from ammonia. *Appl. Catal., B* **2004**, *52*, 287−299.

(23) Li, L.; Zhang, T.; Cai, J.; Cai, H.; Ni, J.; Lin, B.; Lin, J.; Wang, X.; Zheng, L.; Au, C.-T.; Jiang, L. Operando spectroscopic and isotopic-label-directed observation of LaN-promoted Ru/ZrH_2 catalyst for ammonia synthesis via associative and chemical looping route. *J. Catal.* **2020**, *389*, 218−228.

(24) Chen, S.-Y.; Nishi, M.; Chang, A.; Hsiao, W.-C.; Mochizuki, T.; Takagi, H.; Yang, C.-M. Well-ordered Cs-Ru/@SBA-15 nano-composite materials for low pressure ammonia synthesis. *Sustainable Energy Fuels* **2020**, *4*, 5802−5811.

(25) Qiu, J.-Z.; Hu, J.; Lan, J.; Wang, L.-F.; Fu, G.; Xiao, R.; Ge, B.; Jiang, J. Pure Siliceous Zeolite-Supported Ru Single-Atom Active Sites for Ammonia Synthesis. *Chem. Mater.* **2019**, *31*, 9413−9421.

(26) Ma, Y.; Lan, G.; Wang, X.; Zhang, G.; Han, W.; Tang, H.; Liu, H.; Li, Y. Effect of nitrogen co-doping with ruthenium on the catalytic performance of Ba/Ru-N-MC catalysts for ammonia synthesis. *RSC Adv.* **2019**, *9*, 22045−22052.

(27) Wang, X.; Peng, X.; Ran, H.; Lin, B.; Ni, J.; Lin, J.; Jiang, L. Influence of Ru Substitution on the Properties of LaCoO$_3$ Catalysts for Ammonia Synthesis: XAFS and XPS Studies. *Ind. Eng. Chem. Res.* **2018**, *57*, 17375−17383.

(28) Narasimharao, K.; Seetharamulu, P.; Rama Rao, K. S.; Basahel, S. N. Carbon covered Mg-Al hydrotalcite supported nanosized Ru catalysts for ammonia synthesis. *J. Mol. Catal. A: Chem.* **2016**, *411*, 157−166.

(29) Zhang, L.; Lin, J.; Ni, J.; Wang, R.; Wei, K. Highly efficient Ru/Sm$_2$O$_3$-CeO$_2$ catalyst for ammonia synthesis. *Catal. Commun.* **2011**, *15*, 23−26.

(30) Huang, J.; Yuan, M.; Li, X.; Wang, Y.; Li, M.; Li, J.; You, Z. Inhibited hydrogen poisoning for enhanced activity of promoters-Ru/Sr$_2$Ta$_2$O$_7$ nanowires for ammonia synthesis. *J. Catal.* **2020**, *389*, 556−565.

(31) Lin, B.; Liu, Y.; Heng, L.; Ni, J.; Lin, J.; Jiang, L. Effect of ceria morphology on the catalytic activity of Co/CeO$_2$ catalyst for ammonia synthesis. *Catal. Commun.* **2017**, *101*, 15−19.

(32) Hagen, S.; Barfod, R.; Fehrmann, R.; Jacobsen, C. J. H.; Teunissen, H. T.; Chorkendorff, I. Ammonia synthesis with barium-promoted iron-cobalt alloys supported on carbon. *J. Catal.* **2003**, *214*, 327−335.

(33) Lin, B.; Qi, Y.; Wei, K.; Lin, J. Effect of pretreatment on ceria-supported cobalt catalyst for ammonia synthesis. *RSC Adv.* **2014**, *4*, 38093−38102.

(34) Vojvodic, A.; Medford, A. J.; Studt, F.; Abild-Pedersen, F.; Khan, T. S.; Bligaard, T.; Nørskov, J. K. Exploring the limits: A low-pressure, low-temperature Haber-Bosch process. *Chem. Phys. Lett.* **2014**, *598*, 108−112.

(35) Sato, K.; Miyahara, S.-i.; Tsujimaru, K.; Wada, Y.; Toriyama, T.; Yamamoto, T.; Matsumura, S.; Inazu, K.; Mohri, H.; Iwasa, T.; Taketsugu, T.; Nagaoka, K. Barium Oxide Encapsulating Cobalt Nanoparticles Supported on Magnesium Oxide: Active Non-Noble Metal Catalysts for Ammonia Synthesis under Mild Reaction Conditions. *ACS Catal.* **2021**, *11*, 13050−13061.

(36) Miyahara, S.-i.; Sato, K.; Kawano, Y.; Imamura, K.; Ogura, Y.; Tsujimaru, K.; Nagaoka, K. Ammonia synthesis over lanthanoid oxide-supported ruthenium catalysts. *Catal. Today* **2021**, *376*, 36−40.

(37) Sato, K.; Imamura, K.; Kawano, Y.; Miyahara, S.-i.; Yamamoto, T.; Matsumura, S.; Nagaoka, K. A low-crystalline ruthenium nano-layer supported on praseodymium oxide as an active catalyst for ammonia synthesis. *Chem. Sci.* **2017**, *8*, 674−679.

(38) Ogura, Y.; Tsujimaru, K.; Sato, K.; Miyahara, S.-i.; Toriyama, T.; Yamamoto, T.; Matsumura, S.; Nagaoka, K. Ru/La$_{0.5}$Pr$_{0.5}$O$_{1.75}$ Catalyst for Low-Temperature Ammonia Synthesis. *ACS Sustainable Chem. Eng.* **2018**, *6*, 17258−17266.

(39) Kojima, R.; Aika, K.-i. Cobalt molybdenum bimetallic nitride catalysts for ammonia synthesis Part 2. Kinetic study. *Appl. Catal., A* **2001**, *218*, 121−128.

(40) Imamura, K.; Miyahara, S.-i.; Kawano, Y.; Sato, K.; Nakasaka, Y.; Nagaoka, K. Kinetics of ammonia synthesis over Ru/Pr$_2$O$_3$. *J. Taiwan Inst. Chem. Eng.* **2019**, *105*, 50−56.

(41) Kitano, M.; Kujirai, J.; Ogasawara, K.; Matsuishi, S.; Tada, T.; Abe, H.; Niwa, Y.; Hosono, H. Low-Temperature Synthesis of Perovskite Oxynitride-Hydrides as Ammonia Synthesis Catalysts. *J. Am. Chem. Soc.* **2019**, *141*, 20344−20353.

(42) Gao, W.; Wang, P.; Guo, J.; Chang, F.; He, T.; Wang, Q.; Wu, G.; Chen, P. Barium Hydride-Mediated Nitrogen Transfer and Hydrogenation for Ammonia Synthesis: A Case Study of Cobalt. *ACS Catal.* **2017**, *7*, 3654−3661.

(43) Gong, Y.; Wu, J.; Kitano, M.; Wang, J.; Ye, T.-N.; Li, J.; Kobayashi, Y.; Kishida, K.; Abe, H.; Niwa, Y.; Yang, H.; Tada, T.; Hosono, H. Ternary intermetallic LaCoSi as a catalyst for N-2 activation. *Nat. Catal.* **2018**, *1*, 178−185.

(44) Aika, K.; Kubota, J.; Kadowaki, Y.; Niwa, Y.; Izumi, Y. Molecular sensing techniques for the characterization and design of new ammonia catalysts. *Appl. Surf. Sci.* **1997**, *121−122*, 488−491.

(45) Aika, K.-i. Role of alkali promoter in ammonia synthesis over ruthenium catalysts-Effect on reaction mechanism. *Catal. Today* **2017**, *286*, 14−20.

(46) Javaid, R.; Matsumoto, H.; Nanba, T. Influence of Reaction Conditions and Promoting Role of Ammonia Produced at Higher Temperature Conditions in Its Synthesis Process over Cs-Ru/MgO Catalyst. *Chemistryselect* **2019**, *4*, 2218−2224.

(47) Siporin, S.; Davis, R. J. Use of kinetic models to explore the role of base promoters on Ru/MgO ammonia synthesis catalysts. *J. Catal.* **2004**, *225*, 359−368.

(48) Nanba, T.; Nagata, Y.; Kobayashi, K.; Javaid, R.; Atsumi, R.; Nishi, M.; Mochizuki, T.; Manaka, Y.; Kojima, H.; Tsujimura, T.; Matsumoto, H.; Fujimoto, T.; Suzuki, K.; Oouchi, T.; Kameda, S.; Hoshino, Y.; Fujimoto, S.; Kai, M.; Fujimura, Y. Explorative Study of a Ru/CeO$_2$ Catalyst for NH$_3$ Synthesis from Renewable Hydrogen and Demonstration of NH$_3$ Synthesis under a Range of Reaction Conditions. *J. Jpn. Pet. Inst.* **2021**, *64*, 1.